

Observation of many-body dressed molecules

fermi1¹, Arthur Christianen, Richard Schmidt

¹MIT-Harvard Center for Ultracold Atoms,
Research Laboratory of Electronics,
and Department of Physics,
Massachusetts Institute of Technology,
Cambridge, Massachusetts 02139, USA

(Dated: May 29, 2023)

The way the properties of particles change in presence of a background field is an essential topic in various fields of physics. Here we demonstrate that this can also be true in case of chemistry. To this end, we prepare a system of fermionic ^{40}K impurities immersed in a Bose-Einstein condensate of ^{23}Na . For weak interactions the impurities form so-called Bose polarons, which are by now well understood. However, at strong coupling the rules of chemistry enter the game, and the impurity and the bosons can form bound states. We observe the formation of coherent superpositions of dimer and trimer states, which are coupled due to the background condensate. This shows the remarkable role a quantum medium can play in the formation of ultracold molecules. Indeed, this also marks the first observation of heteronuclear Efimov trimer states in the mass-unfavourable regime.

INTRO

In the standard model of physics, many important properties of the elementary particles are defined by their interaction with background fields, e.g., the Higgs field, which gives all particles their mass, or the electromagnetic field, which mediates the forces between charged particles. Cold atom experiments have proven to be clean realizations of tunable model systems, providing insight into this paradigm from a unique perspective. Indeed, one of the foundations of the field was the production and observation of Bose-Einstein condensates (BEC), demonstrating that composite particles too can serve as a background field and be well-described by field theory. As in the standard model, the BEC as a medium can strongly affect the properties of the particles immersed in it. As a concrete example, we consider the case of a fermionic ^{40}K atom in a BEC of ^{23}Na . The quasiparticle which is formed by this “quantum impurity” dressed by the BEC is called the Bose polaron, after the paradigmatic polaron well known in condensed matter.

At weak coupling the Bose polaron is relatively simple to understand: mean-field theory gives a good description and the quasiparticle properties can be expressed in terms of a set of simple universal variables. However, at strong coupling it becomes apparent that in fact the rules of *chemistry* describe the interactions between the impurity atom and the atoms from the BEC. The formation of bound states is crucial in this model, marking a clear difference from typical polarons in condensed matter physics.

In the strong coupling regime, the Bose polaron problem is theoretically challenging due to the presence of many-body bound states and correlations. These kinds of states are usually avoided for a fermionic bath, since Pauli blocking prevents more than one fermionic bath

particle from binding to the impurity. In the bosonic case, only the interboson repulsion prevents infinitely many non-interacting bosons from binding or collapsing onto the impurity. Simultaneously, a mobile impurity can mediate attractive interactions, which instead stimulates binding to the impurity. These mediated interactions for example gives rise to the Efimov effect, the existence of a set of universal trimer states despite interactions being too weak to form a dimer. Our study explores this problem by producing such many-body bound states spectroscopically, and our observations provide an excellent testing ground for modern theory.

We see that the background BEC stimulates the formation of a conceptually new quasiparticle, i.e., a coherent superposition of the dimer, trimer, and free impurity states. This is illustrated in Fig. 1. In Fig. 1a) we qualitatively show the mixture we prepare, with the BEC in orange, the bosonic excitations in red and the impurities in blue. In Fig. 1b) we see an effective emerging three-level Hamiltonian, where the “bare” levels correspond to a free impurity, a dimer and a trimer state, and where the off-diagonal coupling between these levels is caused by the BEC. The eigenvalues of this Hamiltonian and the character of the eigenstates in terms of the different free components is shown in Fig. 1c).

The formation of these superposition state appears since the coupling between the dimer and trimer by the BEC is an order of magnitude larger than their difference in binding energies, in contrast to typical molecular spectroscopy. This provides evidence that the eigenstates we observe are strongly mixed, and amplifies the effect of the higher-order correlations in the system, which would otherwise be extremely challenging to observe. This three level mixing matrix is on the one hand similar to the famous Cabibbo–Kobayashi–Maskawa (CKM) matrix describing the mixing of the quarks in the standard model due to the weak force. On the other hand, our results

show how fundamental concepts of physics can have a remarkable effect on chemical processes in a degenerate medium in the form of molecule formation. These insights can potentially have a strong impact on the way how molecules are created at such cold temperatures, and might suggest an interesting route towards the preparation of trimers.

EXPERIMENTAL DETAILS

The experiment starts with an ultracold gas of fermionic ^{40}K immersed in an ultracold gas of bosonic ^{23}Na , both species jointly trapped in a crossed optical dipole trap (ODT) as ellipsoidal atom clouds in their respective hyperfine ground states ($|F=1, m_F=1\rangle$ for ^{23}Na and $|F=9/2, m_F=-9/2\rangle \equiv |\downarrow\rangle$ for ^{40}K). The Bose-Fermi mixture is sympathetically cooled to temperatures of $\approx 100\text{nK}$ making use of an interspecies three-body zero crossing to minimize losses. After evaporation,

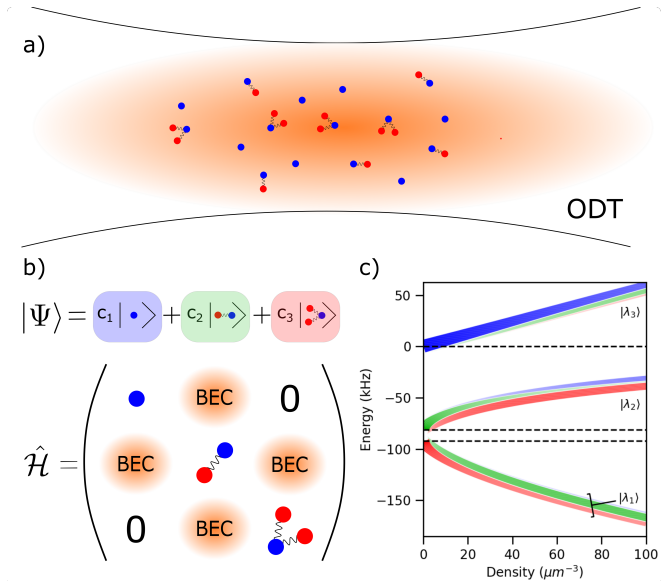


FIG. 1. Pictorial overview of our work. a) The BEC of ^{23}Na (orange), trapped in an optical dipole trap (ODT), containing ^{40}K impurities (blue) after photo-association. Some impurities bind with bosons from the BEC (in red) to form dimers and trimers. b) The wave function of a single impurity in a BEC forming a superposition of a free impurity, a dimer, and a trimer, and the effective Hamiltonian in the basis of these three states. On the diagonal are the energies of these states and the off-diagonal contributions are due to the exchange of particles with the BEC. c) The energies (in kHz) and structure of the three eigenstates $|\lambda\rangle$ of this Hamiltonian as a function of the density of the BEC in μm^{-3} . The widths and opacities of the colored sub-lines indicate the size of the coefficients (as shown in b)) $|c_1|^2$ (blue), $|c_2|^2$ (green) and $|c_3|^2$ (red) for each of the eigenstates. The horizontal dashed lines indicate the energies of the three basis states in absence of a background BEC.

the ODT has trapping frequencies $2\pi \times (108, 112, 9)$ Hz, and the bosons condense into a BEC with a typical peak density of $n_B \approx 40\mu\text{m}^{-3}$ with the fermions deeply in the impurity regime. The condensate is weakly interacting, with an interboson scattering length of $a_{BB} = 52a_0$ where a_0 is the Bohr radius.

To study how the existence of few-body bound states affects the many-body dressing of the impurities immersed in a degenerate bosonic bath, we perform rf injection spectroscopy by driving ^{40}K into a final state $|F=9/2, m_F=-7/2\rangle \equiv |\uparrow\rangle$ that supports shallow bound states in the impurity-boson interatomic potential. By measuring transferred population while varying the drive frequency, we map out the spectrum of the final state's many-body Hamiltonian. We control the final state's interaction strength with the bath using a magnetic Feshbach resonance and use B -fields between 100 and 120G, for which the interspecies scattering length a varies between ~ 500 and $-1800\ a_0$.

An essential feature of our experiment is that the im-

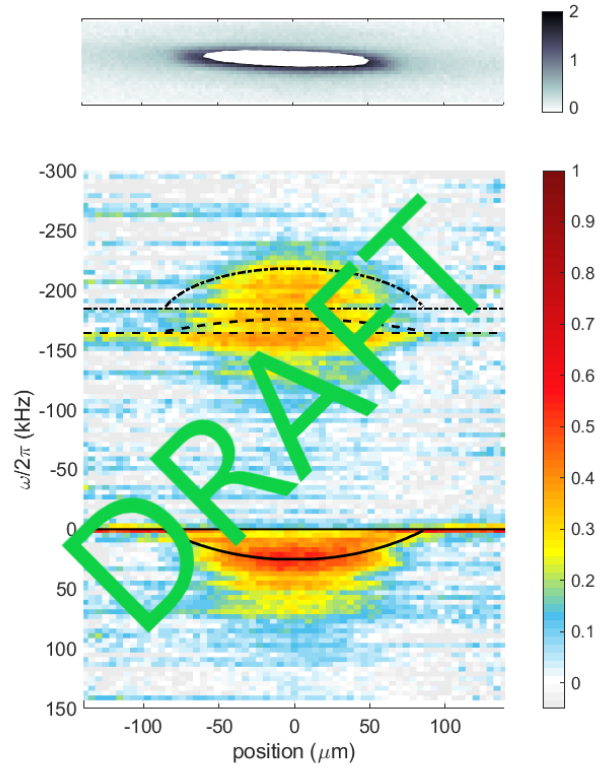


FIG. 2. [FIGURE DRAFT IN PROGRESS] The population transfer from impurity spin state $|\downarrow\rangle$ depends strongly on its position within the BEC. We show spatially resolved spectra at $B = 102.5\text{G}$ measuring the remaining population in $|\downarrow\rangle$ as a function of displacement along the long axis of the cigar shaped trap. Impurities deeply immersed in the BEC show striking deviations from theory predictions only allowing for a single excitation on top of the BEC.

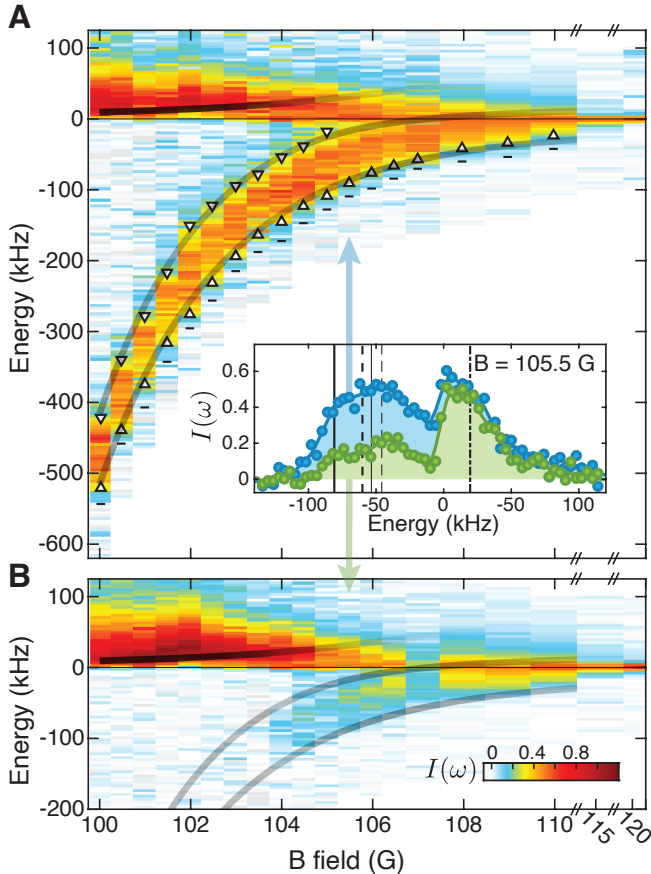


FIG. 3. Measurement of the RF transfer fraction in the center of the BEC via (A) depletion of $|\downarrow\rangle$ and (B) arrival of $|\uparrow\rangle$. Spectra are taken at various magnetic fields and plotted versus the energy of the final state with respect to the bare impurity state. In the inset a cut is shown of the obtained signal at 105.5G. In (A) the full width at half maximum of the signal is indicated by the triangles. The theory results from the three-level model are indicated via the solid lines, of which the opacity is set by the overlap of the states with the initial polaron state, weighted by the duration of the RF pulse. The horizontal black markers in (A) denote the lowest energies for which nonzero rf transfer was measured in our experiment.

purity is strongly interacting with the bath already in the initial state $|\downarrow\rangle$, with approximately constant $(k_n a)^{-1} \sim -1$, where $k_n = (6\pi n_B)^{1/3}$ is the inverse interboson distance, for $100\text{G} < B < 120\text{G}$. Indeed, we allow the impurity to form a strongly interacting attractive Bose polaron by letting it thermalize with the bath for 25ms before performing spectroscopy. This boosts the wavefunction overlap with the bound states of interest in the final many-body Hamiltonian, as the BEC density is already strongly enhanced near the impurity. This allows us to drive the rf transition to final bound states faster than their decay. As a result we are able to both deplete the initial population as well as witness the production and arrival of novel molecular states in our experiment.

To perform rf injection, we drive with frequencies $\sim 26\text{MHz}$ using a broadband, in-vacuum antenna, providing Rabi frequency $\sim 2\pi \times 10\text{kHz}$ on the 40K $|\downarrow\rangle$ to $|\uparrow\rangle$ hyperfine transition in the absence of the condensate. We drive with amplitude-modulated pulses, with the Blackman window ranging from 275 - 1600us. The pulse time is varied with the impurity-bath interaction strength, such that $\sim 50\%$ of the initial polaron $|\downarrow\rangle$ population is injected into the manifold of bound states. This is necessary as the coupling strength between the initial attractive polaron and bound states changes dramatically near the Feshbach resonance. Subsequently, populations are measured via absorption imaging. Details on the spectroscopy procedure can be found in Appendix XX.

RESULTS

A typical injection spectrum from our study can be first broadly separated into two regions, of positive and negative detuning from the bare hyperfine transition $|\downarrow\rangle$ to $|\uparrow\rangle$ in the absence of the bath. The bare transition absorbs energy from the rf drive. Therefore, transfer at negative detuning ($\omega < 0$) provides information about transitions into bound states; we call this the *attractive polaron* branch. In the few-body or equivalently low density limit, this branch corresponds primarily to the two-body bound state, i.e. Feshbach molecules of NaK. Transfer at positive detuning ($\omega > 0$) indicates an effective repulsion between the impurity and the bath particles. This leads to a local density decrease of the BEC around the impurity, and thus the formation of a *repulsive polaron*. The effective repulsion originates from the need for the eigenstates of the Hamiltonian to be orthogonal to the shallow bound state giving rise to the attractive polaron branch. Both of these branches can be seen in the spectra shown in Fig. 2.

The spatial variation in density of the bath due to the harmonic trapping potential has a strong effect on the resulting transfer $I(\omega)$. We show an example of this in Fig. 2 by spatially resolving the spectra. In the attractive polaron branch of the spectra, we make two key experimental observations that emerge as the boson density increases near the center of the BEC. First, the initial state couples into states more deeply bound than the dimer, and second, the spectroscopic feature broadens well above both the frequency resolution of the rf probe and the energy scale of the sample temperature.

Neither of these observations can be simply explained in a two-body picture. The theoretical polaron energy when limiting the calculation to at most one excitation on top of the BEC is shown as the dashed line, clearly failing to account for the main spectral feature. Instead, the role of three-body and many-body physics is crucial to understand our system in the high density regime. First, we note that in the three-body limit, an Efimov trimer

state of Na + Na + K exists near the Na + K dimer state, as is shown by the two lower dashed lines in Fig. 1C. Furthermore, the presence of a condensate strongly coupled to the impurities has two effects. The background field strongly mixes the dimer and trimer states, leading to level repulsion in the effective three-level system (solid curves of Fig. 1C) and modified decay lifetimes arising from admixture of the lossy trimer state. Finite lifetimes however are insufficient to explain the spectral widths, and thus we infer that the impurity arrives at an energy landscape that is intrinsically broad due to coupling with a dense bath.

To understand the effects of the existence of two- and three-body bound states along with the presence of a dense BEC, we use the double excitation approach as described in Ref. ..., with minor modifications. In brief, we use a single channel model with Gaussian model potentials for both the boson-impurity and boson-boson scattering. We fix the scattering length and effective range to the values found from full coupled-channels solutions of the two-body problem using realistic potentials from Refs. [1, 2]. The interboson repulsion is treated fully close to the impurity, and using the Born approximation far from the impurity. We take a variational approach as shown in Fig. 1b), allowing zero, one, or two excitations from the background condensate. We optimize the wave functions in these sectors to minimize the ground state energy of the coupled problem, and then use these wave functions to construct the simplified Hamiltonian in Fig. 1b). Thus, we have obtained our three-level model including the two excited states. None of the model parameters are fitted to the experimental results obtained in this work. Further details can be found in Appendix XX.

In Fig. 3 we see the polaron rf-spectrum as a function of the magnetic field, studying our system over a broad range of impurity-bath final interaction strengths. Focusing first on Fig. 3A, we show the spectrum obtained from measuring the atoms transferred from the initial state, and we see again the repulsive and attractive polaron branches. The black horizontal bars in Fig. 3A mark the deepest binding energies where we see spectral response, and the threshold behavior we observe on the low-energy flank of the spectra strongly suggests that we indeed observe the ground state of the final state Hamiltonian. The full width at half maximum (FWHM) of the attractive branch is indicated by the triangles, and the theory curves (opaque lines) are computed using the three-level model discussed before. The opacity of the theory curves is given by the overlap of the initial state and weighted by the rf pulse length T_{rf} , which is proportional to the transferred population for pulses within linear response. We additionally note that for $B = 115, 120$ G, the interspecies scattering length of initial and final spin states are approximately equal, so despite strong interactions, both branches collapse into a single feature

given by the spectral resolution of our probe.

Our theoretical models reliably describe the FWHM frequencies of the attractive polaron branch over the wide range of interaction strengths explored. Both the lower edge of the spectrum agrees well with the ground state from the double excitation model, but also the upper edge of the spectrum agrees well with the second state in our three-level model. This indicates that an essential mechanism setting the width of the spectrum is the BEC-induced coupling between the different “bare” particle-number bound states, as shown by the off-diagonal matrix elements in Fig.1B. Our models accounting for the many-body correlations due to the BEC are sufficient to predict the spectral location and width, but the accurate computation of the full spectral lineshapes is beyond current theoretical approaches. Our experiment provides an excellent testbed for developing theory that also includes the mechanisms of three-body loss and adding phononic excitations on top of the molecular states.

We remark that the peaks of the repulsive polaron branch of the spectra deviate from its theoretical repulsion energy, as shown by the upper opaque line in Fig.3A. This is however unsurprising since the spectral weight depends not only the available density of states, but also the wavefunction overlap between states. The overlap of the attractive polaron with the repulsive polaron state decreases with increasing impurity-boson repulsion. The overlap in this case is stronger with the levels below the repulsive polaron state.

We can compare the depletion signal from Fig. 3A to Fig. 3B, where we show the number of arrived atoms in the final state. A quantitative analysis allows us to infer the decay lifetimes $1/\Gamma$ of the states prepared during the rf injection pulse time. We model transfer between populations P_\downarrow, P_\uparrow as $dP_\downarrow \propto -\Omega_R(t)^2 P_\downarrow dt$, where the Rabi frequency Ω_R is time-dependent due to pulse shaping, and the loss in $|\uparrow\rangle$ as $dP_\uparrow + dP_\downarrow = -\Gamma P_\uparrow dt$. We first are able to observe the arrival of the upper repulsive polaron branch, where losses are weak. However, in the attractive branch the arrival signal is much weaker. The origin of this effect is the final state being short-lived compared to the rf pulse duration. It is no surprise that the final states are short lived, since they are predicted to contain a large trimer fraction, and the trimers have a short lifetime due to three-body recombination. We find that the lifetime decreases substantially with increasing binding energy. Qualitatively this is to be expected, since the probability that the three particles meet each other at short distance and undergo the recombination reaction increases along with the binding energy.

CONCLUSION/OUTLOOK

Our study provides experimental observation of conceptually novel molecular states in a superposition of

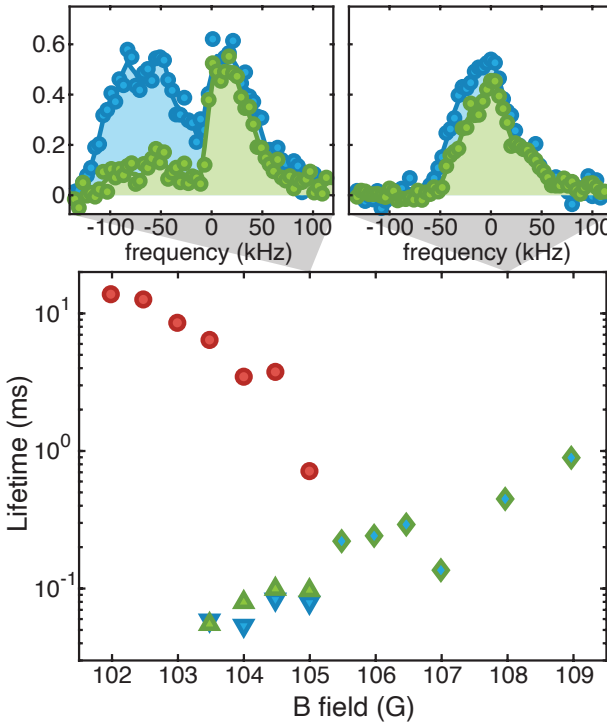


FIG. 4. The lifetimes of the states created by rf injection are inferred from the ratio of population depleted from $|\downarrow\rangle$ to population observed in $|\uparrow\rangle$, as shown in Fig. 3. Population transferred to $|\uparrow\rangle$ during the rf pulse can decay rapidly due to three-body recombination. For data taken at $B \leq 105\text{G}$, we are able to resolve the attractive and repulsive branches of the spectrum, whereas for larger magnetic fields the two features merge. This can be seen in the exemplary spectra shown in the top row. The lifetime of the bound states (triangles) decreases at deeper binding energy (away from the Feshbach resonance), whereas the lifetime of the repulsive polaron branch (circles) increases. At sufficiently deep binding energies, we do not observe any population in $|\downarrow\rangle$.

two- and three-body bound states, induced by coupling to a degenerate bosonic bath. We find that the mixing induced by the background field causes strong level repulsion, setting one of the dominant energy scales in our spectra. We show that by preparing an initial metastable polaronic state, we are able to probe the unexplored crossover between few- and many-body physics of fermions immersed in a BEC within experimentally meaningful timescales. Furthermore, our measurements provide an excellent testing ground for both existing and developing theories of polaron systems.

Our work opens the door into several new directions, spanning from fundamental questions on the role of quantum coherence in polaron physics to the present challenges in ultracold atomic and molecular gases. There are conflicting theoretical results on the finite temperature properties of the Bose polaron, and it remains to be explored to which degree the coherence that accompa-

nies the high density and low temperature of the bosonic bath is essential to observing the CKM-like hybridization effects. Such experiments could be implemented cleanly in homogeneous trapping potentials, where the spatial density is decoupled from temperature. We separately raise the experimental question of whether the existence and proximity of few-body bound states is a fundamentally limiting loss mechanism on the road to efficient creation and quantum degeneracy of molecular gases, when starting from degenerate atomic quantum mixtures near a Feshbach resonance [cite experimental papers]. We shed light on this process with spectroscopic precision by revealing many-body correlations and finite final state lifetimes of impurities immersed in a quantum bath.

APPENDIX: "COMPLETE" THEORY DESCRIPTION

[Complete version of the theory, of course needs to be shortened for main text]

General

We consider the problem of an impurity of mass M in a homogeneous BEC of bosons with mass m and chemical potential μ_U . We denote the impurity-boson interaction potential by V_{IB} and the boson-boson interaction potential by V_{BB} . We treat the impurity in first quantization with quadrature operators $\hat{\mathbf{R}}$ and $\hat{\mathbf{P}}$, and the bosons in second quantization with creation and annihilation operators \hat{b}_k^\dagger and \hat{b}_k . This gives the following Hamiltonian

$$\begin{aligned} \hat{\mathcal{H}}_0 = & -E_{bg} + \int d^3k \left(\frac{k^2}{2m} - \mu_U \right) \hat{b}_k^\dagger \hat{b}_k + \frac{\hat{P}^2}{2M} \\ & + \int d^3r V_{IB}(\mathbf{r} - \hat{\mathbf{R}}) \hat{b}_r^\dagger \hat{b}_r + \frac{1}{2} \int \int d^3r' d^3r' V_{BB}(\mathbf{r}' - \mathbf{r}) \hat{b}_{r'}^\dagger \hat{b}_{r'}^\dagger \hat{b}_{r'} \hat{b}_{r'}. \end{aligned} \quad (1)$$

Here E_{bg} is the energy of the background BEC without the impurity. We set the total momentum of the system to zero, and the chemical potential to $\mu_U = n_0 \int d^3r V_{BB}(\mathbf{r})$. To approximate the ground state of the Hamiltonian we consider a variational Ansatz of the type

$$|\psi\rangle = \hat{U}_{n_0} \hat{U}_{LLP} \hat{A}(\mathbf{x}) |0\rangle, \quad (2)$$

where the unitary \hat{U}_{n_0} displaces the background condensate approximated by a coherent state and \hat{U}_{LLP} , given by:

$$\hat{U}_{LLP} = \exp(-i\hat{\mathbf{R}} \int dk \mathbf{k} \hat{b}_k^\dagger \hat{b}_k), \quad (3)$$

performs the Lee-Low-Pines transformation to transform to the reference frame of the impurity. The operator $\hat{A}(\mathbf{x})$ dependent on variational parameters \mathbf{x} is optimized to minimize the energy, and $|0\rangle$ is the bosonic vacuum state with the impurity at the center of the frame.

$$\begin{aligned}\hat{\mathcal{H}} = & \hat{U}_{LLP}^\dagger \hat{U}_{n_0}^\dagger \hat{\mathcal{H}}_0 \hat{U}_{n_0} \hat{U}_{LLP} = \int d^3k \frac{k^2}{2\mu_r} \hat{b}_k^\dagger \hat{b}_k \\ & + \frac{1}{2M} \int \int d^3k' d^3k' \mathbf{k}' \hat{b}_{\mathbf{k}'}^\dagger \hat{b}_{\mathbf{k}'}^\dagger \hat{b}_{\mathbf{k}'} \hat{b}_{\mathbf{k}'} \\ & + \int d^3r V_{IB}(\mathbf{r}) (\hat{b}_r^\dagger + \sqrt{n_0}) (\hat{b}_r + \sqrt{n_0}) \\ & + \int \int d^3r' d^3r' V_{BB}(\mathbf{r}' - \mathbf{r}) [\frac{n_0}{2} (2\hat{b}_{\mathbf{r}'}^\dagger \hat{b}_{\mathbf{r}'} + \hat{b}_{\mathbf{r}'}^\dagger \hat{b}_{\mathbf{r}'}^\dagger + \hat{b}_{\mathbf{r}'} \hat{b}_{\mathbf{r}'}^\dagger) \\ & + \sqrt{n_0} (\hat{b}_{\mathbf{r}'}^\dagger \hat{b}_{\mathbf{r}'}^\dagger \hat{b}_{\mathbf{r}'} + \hat{b}_{\mathbf{r}'}^\dagger \hat{b}_{\mathbf{r}'} \hat{b}_{\mathbf{r}'}^\dagger) + \frac{1}{2} \hat{b}_{\mathbf{r}'}^\dagger \hat{b}_{\mathbf{r}'}^\dagger \hat{b}_{\mathbf{r}'} \hat{b}_{\mathbf{r}'}].\end{aligned}\quad (4)$$

We take a double excitation Ansatz (DEA)

$$\begin{aligned}\hat{A}[\beta_0, \beta(\mathbf{k}), \alpha(\mathbf{k}, \mathbf{k}')] = & \beta_0 + \int d^3k \beta(\mathbf{k}) \hat{b}_k^\dagger \\ & + \int \int d^3k d^3k' \alpha(\mathbf{k}, \mathbf{k}') \hat{b}_k^\dagger \hat{b}_{\mathbf{k}'},\end{aligned}\quad (5)$$

To facilitate numerical implementation, we parametrize the momentum dependent functions as

$$\beta(\mathbf{k}) = \sum_i \beta_i \chi_i(\sigma_{\beta,i}, \mathbf{k}), \quad (6)$$

$$\alpha(\mathbf{k}, \mathbf{k}') = \sum_{ij} A_{ij} \chi_i(\sigma_{\alpha,i}, \mathbf{k}) \chi_j(\sigma_{\alpha,j}, \mathbf{k}), \quad (7)$$

$$(8)$$

where the indices i are shorthand for (nlm) and the functions $\chi_i(\sigma, \mathbf{k})$ are spherical Gaussian basis functions,

$$\chi_{lm}(\sigma, \mathbf{k}) = Y_{lm}(\theta, \phi) k^l \exp(-\sigma k^2). \quad (9)$$

Potentials

We take potentials of the form

$$V_{IB}(\mathbf{r}) = \frac{g}{2L_g^2} \exp\left(-\frac{r^2}{L_g^2}\right), \quad (10)$$

$$V_{BB}(\mathbf{r}) = \frac{U_1}{2L_{U1}^2} \exp\left(-\frac{r^2}{L_{U1}^2}\right) + \frac{U_2}{2L_{U2}^2} \exp\left(-\frac{r^2}{L_{U2}^2}\right). \quad (11)$$

To fix g and L_g we fix the following procedure. We compute the scattering length and effective range with coupled channels calculations as a function of the magnetic field using the potentials from Ref. [2]. Then for

every magnetic field we change g and L_g as to reproduce these parameters.

For the interboson repulsion the scattering length and effective range only experience a negligible variation over the magnetic field range of study. We compute the interboson scattering length and effective range using coupled channels calculations using potentials from Ref. [1] at $B = 105$ Gauss. Unfortunately, the found combination of scattering length and effective range can not be achieved with a single Gaussian potential. Therefore we use a sum of two Gaussian potentials. However, in this case there is no unique choice. We therefore compute the trimer energies for several of these interboson potentials and then the found difference in energy can be treated as an estimate of the uncertainty. Note that there is not a single parameter which is fitted explicitly to the experimental data.

What is challenging with this approach is to get a good resolution for the interboson scattering far away from the impurity. The idea now is to treat the scattering far from the impurity on the level of the Born approximation, and only treat the full scattering close to the impurity.

Therefore we approximate the interboson repulsion energy with the following energy functional:

$$\begin{aligned}E_U(\beta_0, \beta, \alpha) \approx & \sum_{i=1,2} \frac{1}{2L_{Ui}^2} \int \int d^3r d^3r' \exp\left[-\frac{(\mathbf{r}' - \mathbf{r})^2}{L_{Ui}^2}\right] \left\{ \frac{n_0 U_{Bi}}{2} [2\beta^*(\mathbf{r})\beta(\mathbf{r}')] \right. \\ & + 4 \int d\mathbf{r}'' \alpha^*(\mathbf{r}', \mathbf{r}'') \alpha(\mathbf{r}'', \mathbf{r}) + h.c. \left. \right\} \\ & + \sqrt{2n_0} U_{Bi} [\beta^*(\mathbf{r})\alpha(\mathbf{r}, \mathbf{r}') + h.c.] + U_{Bi} |\alpha(\mathbf{r}', \mathbf{r})|^2 \\ & + \exp\left[-\frac{(\mathbf{r}' - \mathbf{r})^2}{L_{Ui}^2} - \frac{\mathbf{r}'^2 + \mathbf{r}^2}{L_W^2}\right] (U_i - U_{Bi}) |\alpha(\mathbf{r}', \mathbf{r})|^2\end{aligned}\quad (12)$$

Here L_W is fixed by the following procedure: we assume that to get a proper description L_W should scale linearly with the range of the interboson potential, the range we choose to use here is the classical turning point. To determine the prefactor we compare various potentials with the same scattering length and effective range, and postulate that the energy of the trimer state should be the same close to unitarity. The result is shown in Fig.3. Here the difference between the dimer and trimer energies is shown from various theoretical calculations. The dots correspond to experimental results.

The red and black curves show the result for six different potentials where the three-body problem is solved without replacing the interaction with the effective three-body interaction with our model with a fixed basis set. One sees here a large difference between the different curves. The cyan and green curves show what happens after our procedure: all the curves collapse on top of each

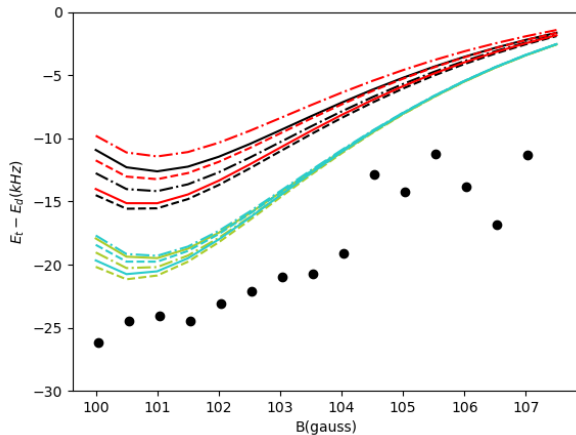


FIG. 5. [Will update the figure, but this is what it qualitatively looks like]

other for weak binding energies and only differ from each other at stronger interactions. Note that the value of L_W found depends on the computational basis set.

For the trimer energy there is a difference between the theoretical and experimental results. This could have the following reasons:

1. Multichannel effects: effect of proximity of other resonances (this is not an isolated resonance)
2. Experimental resolution is limited, due to broadening and three-body loss
3. Theoretical description is still not complete

Three-level model

In principle one can extract a whole spectrum from the DEA method. However:

1. For this the parametrization in terms of Gaussian basis set is not good
2. DEA misses effects which are not so important for the ground state energy but more important for the spectrum: dressing of the molecular state by long range polaron cloud / phononic excitations in both initial and final state.
3. No three-body loss is included

To still get a qualitative feeling, we came up with our three-level model. In this model we do not extract the entire spectrum but only three lines which should present the qualitative features. What we do is the following: we first find the ground state energy and wave function from the DEA. From the DEA we have a dimer and a trimer wave function. Then we restrict the Hilbert space to the space where the bare states are the free impurity, this dimer and this trimer. This Hamiltonian we then diagonalize. The lowest state then corresponds exactly to the DEA result, but this way we also get two excited states.

As can be seen: the lower two states nicely describe the width of the continuum into which the dimer and trimer states split. The higher state represents the repulsive polaron, but we do not believe this to be particularly accurate. From this three level model we cannot only extract the energies but also the contributions of the different parts of the wavefunction for each eigenstate and the overlaps of these states with the initial polaron state.

-
- [1] S. Knoop, T. Schuster, R. Scelle, A. Trautmann, J. Appmeier, M. K. Oberthaler, E. Tiesinga, and E. Tiemann, Phys. Rev. A **83**, 042704 (2011).
- [2] T. Hartmann, T. A. Schulze, K. K. Voges, P. Gersema, M. W. Gemel, E. Tiemann, A. Zenesini, and S. Ospelkaus, Phys. Rev. A **99**, 032711 (2019).

APPENDIX: SPECTROSCOPY AND DETECTION

To suppress the spectral sidelobes beyond the Fourier window $1/T_{rf} < 4\text{kHz}$ due to a finite rf pulse time $T_{rf} \geq 275\mu\text{s}$, we amplitude modulate the pulse with a Blackman window function, with parameter $\alpha = 0.16$. The Rabi frequency in the absence of the condensate as a function of time is then $\Omega_{Rabi}(t) = \Omega_{max}((1 - \alpha)/2 - \cos(2\pi t/T_{rf})/2 + \alpha \cos(4\pi t/T_{rf})/2)$ with $\alpha = 0.16$ and $\Omega_{max} \sim 2\pi \times 10 \text{ kHz}$. To measure the populations in each spin state $|\downarrow\rangle$ and $|\uparrow\rangle$ we perform on-resonant absorption imaging, using the corresponding σ_+ transitions to the $40\text{K } P_{3/2}, F' = 11/2$ excited state hyperfine manifold. Each probe is also sensitive to the population in the complementary state, due to off-resonant scattering. We avoid contaminating the measurement of small populations in $|\uparrow\rangle$ (fraction $\lesssim 0.1$) by shelving $|\uparrow\rangle$ to an auxiliary ground hyperfine state during imaging, as described in Appendix XX.

For our relevant experimental parameter regime, the detuning to linewidth ratio is $\Delta/\Gamma \approx 17\text{MHz}/6\text{MHz} \approx 2.8$, which corresponds to an off-resonant scattering cross-section of $\sigma = \sigma_0/(1 + 4(\Delta/\Gamma)^2) \approx 0.03\sigma_0$, for on-resonant cross-section σ_0 .

We shelve the $|\downarrow\rangle$ population to an auxiliary ground hyperfine state $|F = 7/2, m_F = -7/2\rangle \equiv |\text{aux}\rangle$ to eliminate the contamination of the $|\uparrow\rangle$ imaging signal due to off-resonant scattering of $|\downarrow\rangle$. This is done before probing the population in $|\uparrow\rangle$, and afterwards the population in $|\text{aux}\rangle$ is returned to $|\downarrow\rangle$ for imaging. This shelving procedure is designed to cleanly probe small (fraction $\lesssim 0.1$) populations in $|\uparrow\rangle$, whereas measuring the typical populations in $|\downarrow\rangle$ (fraction $\gtrsim 0.5$) is much less demanding.

The $1/e$ lifetime of the lower energy dimer-trimer dressed state is tens of us, constraining the time available for the shelving procedure. Thus, we implement

shelving within 10us by using an optical Raman transition via the excited 40K $P_{1/2}$ state, with a maximum two-photon Rabi frequency $\gg 500\text{kHz}$, one-photon detuning $\approx 20\text{GHz}$. Both the pump and Stokes coupling derive from a single spatial mode near-resonant beam propagating normal to the quantization B-field, with two temporal frequencies satisfying the two-photon resonance condition between $|\uparrow\rangle$ and $|\text{aux}\rangle$.

The optical shelving pulse is configured for insensi-

tivity to pulse timing and two-photon resonance frequency shifts. We adiabatically chirp the two-photon detuning over 2.5 MHz and amplitude modulate the two-photon Rabi frequency with a Blackman window function. This procedure maps to a rapid adiabatic passage in the approximate two-level system spanning $|\uparrow\rangle, |\text{aux}\rangle$ [cite Bergmann Perspective]. The round-trip fidelity of shelving and returning the population was measured to be 0.99 by probing the population in $|\downarrow\rangle$ after up to five round-trips, in the absence of the bath.